

Magnetic dipole sequences in ^{83}Rb

R. Schwengner,¹ G. Rainovski,² H. Schnare,^{1*} A. Wagner,¹ S. Frauendorf,^{1,3} F. Dönaу,¹ A. Jungclaus,⁴ M. Hausmann,⁵ O. Yordanov,⁶ K. P. Lieb,⁵ D. R. Napoli,⁷ G. de Angelis,⁷ M. Axiotis,⁷ N. Marginean,⁸ F. Brandolini,⁹ and C. Rossi Alvarez⁹

¹*Institut für Strahlenphysik, Forschungszentrum Dresden-Rossendorf, D-01314 Dresden, Germany*

²*Faculty of Physics, University of Sofia, BG-1164 Sofia, Bulgaria*

³*Department of Physics, University of Notre Dame, Notre Dame, Indiana 46556, USA*

⁴*Instituto de Estructura de la Materia, Consejo Superior de Investigaciones Científicas, E-28006 Madrid, Spain*

⁵*II. Physikalisches Institut, Universität Göttingen, D-37073 Göttingen, Germany*

⁶*Institute for Nuclear Research and Nuclear Energy, BAS, BG-1784 Sofia, Bulgaria*

⁷*INFN, Laboratori Nazionali di Legnaro, I-35020 Legnaro, Italy*

⁸*Horia Hulubei National Institute of Physics and Nuclear Engineering, Bucharest, P. O. Box MG-6, Romania*

⁹*INFN and Dipartimento di Fisica dell'Università di Padova, I-35131 Padova, Italy*

(Received 21 April 2009; published 8 October 2009)

High-spin states in ^{83}Rb were populated in the reaction $^{11}\text{B} + ^{76}\text{Ge}$ at beam energies of 45 and 50 MeV. γ rays were detected with the spectrometer GASP. The level scheme of ^{83}Rb was extended up to 13.9 MeV. Mean lifetimes of 23 levels were determined using the Doppler-shift-attenuation method. Among the bands newly established is a sequence comprising intense $M1$ transitions and crossover $E2$ transitions. This sequence turns out to be irregular and thus shows that magnetic rotation as observed in the neighboring odd-odd isotopes is not realized in this odd-even nuclide. Excited states in ^{83}Rb were interpreted in terms of the shell model using the model space $\pi(0f_{5/2}, 1p_{3/2}, 1p_{1/2}, 0g_{9/2}) \nu(1p_{1/2}, 0g_{9/2})$. The configurations predicted for the negative-parity $M1$ sequence reproduce the $M1$ transition strengths fairly well.

DOI: [10.1103/PhysRevC.80.044305](https://doi.org/10.1103/PhysRevC.80.044305)

PACS number(s): 23.20.Lv, 25.85.Ge, 27.50.+e

I. INTRODUCTION

Level sequences comprising strong magnetic dipole ($M1$) transitions have been a subject of interest for a long time. First discovered in ^{81}Kr [1,2], they were also observed in the isotopes $^{79,83}\text{Kr}$ [3,4], in the neighboring odd- N nuclide ^{83}Sr [5], and in the odd- Z nuclides $^{77,79,81}\text{Br}$ [6–9] and $^{79,81,83,85}\text{Rb}$ [10–13]. At that time, the strong $M1$ transitions were interpreted in the framework of a semiclassical coupling scheme for the spins of the involved nucleons [1,2]. In nuclei with $N \leq 44$ having quadrupole deformations of $\epsilon_2 \approx 0.20$ – 0.25 , the $M1$ sequences, appearing at about 2.5-MeV excitation energy, coexist with collective rotational bands built on the ground state or on low-lying states and comprising intense quadrupole ($E2$) transitions and weak or no $M1$ transitions [8].

Later on, regular rotational bands with $\Delta J = 1$ and predominating $M1$ transitions were observed in nearly spherical Pb isotopes, where they occur on top of irregular level schemes [14–22]. These so-called shears bands were described in the tilted-axis-tilting (TAC) model and represent a novel rotational mode called magnetic rotation [23]. The TAC model predicts magnetic rotation for several regions of the nuclear chart [24,25]. Indeed, shears bands were also confirmed in the predicted regions around $A = 110$ [26–30] and $A = 140$ [31].

To search for magnetic rotation in the mass $A = 80$ region we studied the Rb isotopes with neutron numbers $N = 45, 46, 47$ and identified $M1$ bands in each of these isotopes. The $M1$ bands in the odd-odd isotopes $^{82}\text{Rb}_{45}$ and $^{84}\text{Rb}_{47}$ follow the regular rotational behavior [$E \sim J(J+1)$,

i.e., $E_\gamma(M1) = \hbar\omega \sim J$] [32,33]. The $B(M1)/B(E2)$ ratios determined from branching ratios of transitions within the $M1$ bands reach values up to 25 $(\mu_N/eb)^2$ and decrease smoothly with increasing spin in the range of $13 \leq J \leq 16$. This behavior is typical for magnetic rotation and caused by the gradual alignment of the spins of the involved proton and neutron orbits (shears mechanism). We described the regular negative-parity $M1$ bands in ^{82}Rb and ^{84}Rb within the TAC model on the basis of the lowest-lying four-quasiparticle (4qp) configuration with negative parity: $\pi(fp)\pi(g_{9/2}^2)\nu(g_{9/2})$ [32,33]. The good agreement between experimental and calculated characteristics proves the validity of the concept of magnetic rotation for these bands.

High-spin states in ^{83}Rb , the even- N isotope between the two odd-odd nuclei ^{82}Rb and ^{84}Rb , had previously been studied via the reactions $^{81}\text{Br}(\alpha, 2n)$, $^{70}\text{Zn}(^{16}\text{O}, p2n)$, $^{74}\text{Ge}(^{12}\text{C}, p2n)$, $^{80}\text{Se}(^6\text{Li}, 3n)$ [34], $^{68}\text{Zn}(^{18}\text{O}, p2n)$, and $^{59}\text{Co}(^{28}\text{Si}, 2p)$ [35]. In the course of the present work we learned about a study of ^{83}Rb using the $^{76}\text{Ge}(^{11}\text{B}, 4n)$ reaction [36]. A sequence of four intense $M1$ transitions linking $13/2^-$ to $21/2^-$ states was found [34] which shows a rotational-like behavior and was described within the TAC model [37]. In the present study we extended the known level sequences to higher spins, established two additional level sequences, and determined 23 level lifetimes applying the Doppler-shift attenuation (DSA) method. Preliminary results of the present study were published in Refs. [12,38,39].

II. EXPERIMENTAL METHODS AND RESULTS

Excited states of ^{83}Rb were populated via the reaction $^{76}\text{Ge}(^{11}\text{B}, 4n)$ using the ^{11}B beam of the XTU tandem

*Present address: Globalfoundries, D-01109 Dresden, Germany.

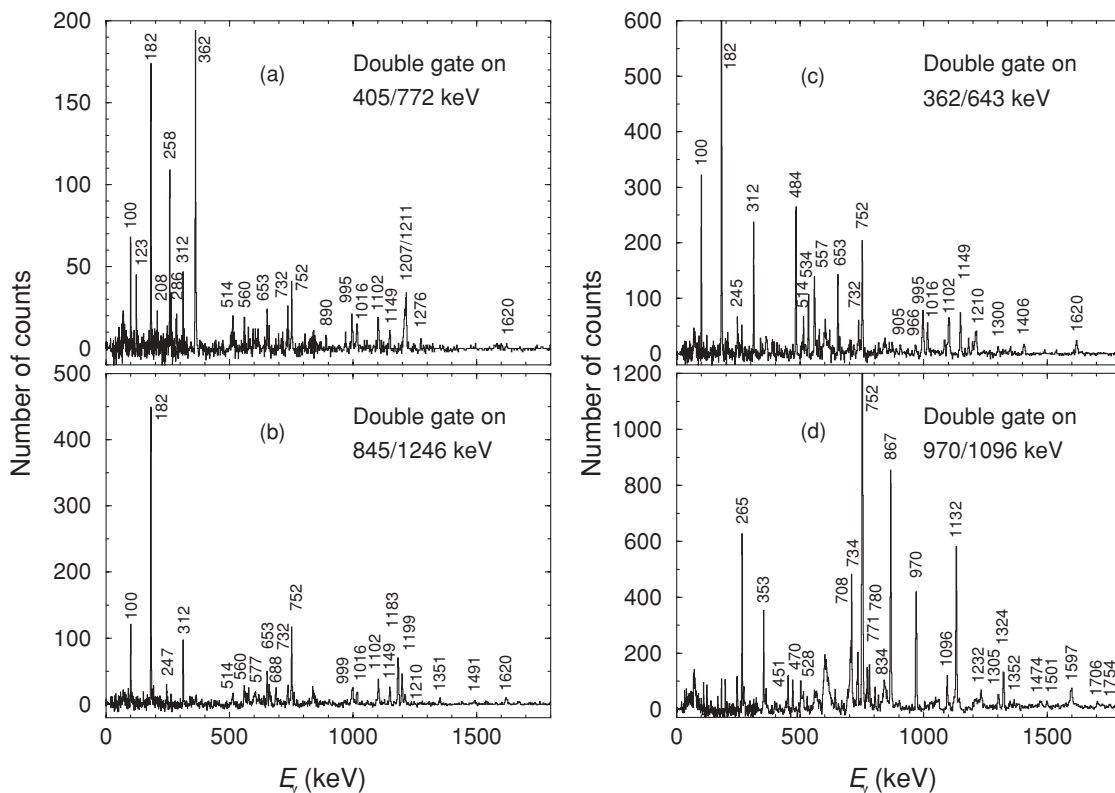


FIG. 1. Examples of doubly gated coincidence spectra. Transitions assigned to ^{83}Rb are marked with their energies in keV.

accelerator of the Laboratori Nazionali di Legnaro. γ rays were detected with the GASP spectrometer [40] consisting of 40 escape-suppressed HPGe detectors and an inner ball containing 80 BGO elements. In the first of the two experiments the beam energy was 50 MeV. A thin target consisting of a stack of two self-supporting ^{76}Ge foils enriched to 92.8% with a thickness of 0.2 mg cm^{-2} each was used. Approximately 1.5×10^8 γ - γ - γ coincidence events were collected and sorted off-line into E_γ - E_γ matrices as well as an E_γ - E_γ - E_γ cube. The beam energy in the second experiment was 45 MeV. The target consisted of a 1.2 mg cm^{-2} thick layer of ^{76}Ge evaporated onto a 3 mg cm^{-2} tantalum backing. A total of 2×10^9 γ - γ coincidence events were measured and sorted off-line into E_γ - E_γ matrices. Coincidence spectra were extracted by setting gates on appropriate peak and background intervals in the cube and the matrices using the Radware package [41] and the code VS [42], respectively. Examples of doubly gated background-corrected coincidence spectra extracted from the cube are shown in Fig. 1. The γ rays assigned to ^{83}Rb on the basis of the present coincidence experiments are compiled in Table I.

A. γ - γ directional correlations

The analysis of directional correlations of coincident γ rays emitted from oriented states (DCO) was applied to deduce multipole orders of γ rays and thus to assign spins to the emitting states. This method is based on the

formalism described in Refs. [43,44] and discussed, e.g., in Ref. [45].

In the present experiment, γ - γ events with one γ ray detected in 1 of the 12 detectors positioned at angles of 31.7° , 36.0° , 144.0° , and 148.3° (weighted averages 35° or 145° , respectively), and the other one detected in 1 of the 8 detectors at 90° relative to the beam direction were sorted into a coincidence matrix. Coincidence spectra were extracted by setting gates on certain peak and background intervals in the ($35^\circ/145^\circ$, 90°) matrix and in the transposed (90° , $35^\circ/145^\circ$) matrix. The DCO ratios were obtained as the ratios of peak intensities in both background-corrected spectra. A DCO ratio of 1.0 is expected if the gating and observed transitions are stretched transitions of pure and equal multipole order, i.e., dipole-dipole or quadrupole-quadrupole. For the present detector geometry and completely aligned nuclei, a value of 0.54 is expected for a pure dipole transition gated on a stretched quadrupole transition. Consequently, the inverse value of 1.85 is expected for a quadrupole transition gated on a dipole transition. The DCO ratios deduced for transitions in ^{83}Rb are listed in Table I.

B. Lifetimes

Mean lifetimes were determined from Doppler shifts of γ rays observed in coincidence spectra at average angles of 35° and 145° to the beam applying the DSA method in connection with the thick target used in the experiment at 45 MeV. The coincidence spectra were extracted from two

TABLE I. γ rays assigned to ^{83}Rb .

E_γ^a (keV)	I_γ^b	R_{Dco}^c	$E_\gamma^{\text{GATE}d}$ (keV)	$\sigma\lambda^e$	$J_i^{\pi f}$	$J_f^{\pi g}$	E_i^h (keV)
100.1(1)	15.2(5)	1.07(7)	182/362	$M1$	$15/2^-$	$13/2^-$	2413.7
103.3(1)	2.4(1)	2.7(10)	182/362	$(M1)$	$17/2^-$	$17/2^-$	2699.4
123.1(2)	5.7(2)	0.82(12)	752	$M1/E2$	$17/2^-$	$15/2^-$	2699.4
176.5(2)	1.3(1)	1.05(40)	182/362	$(M1)$	$17/2^-$	$17/2^-$	2772.5
181.9(1)	43.8(13)	0.60(4)	752	$M1$	$17/2^-$	$15/2^-$	2595.9
196.5(2)	2.0(1)				$21/2^-$	$21/2^-$	3559.3
207.7(3)	2.0(1)	0.87(8)	182/362	$(E1)$	$15/2^-$	$15/2^+$	2413.7
211.2(3)	0.7(1)				$13/2^-$	$13/2^-$	2313.4
237.2(3)	1.0(1)	2.17(24)	182/362	$(M1)$	$19/2^-$	$19/2^-$	3194.3
238.1(2)	1.5(1)				$21/2^-$	$21/2^-$	3600.6
245.0(2)	2.5(1)	0.84(12)	752	$M1/E2$	$11/2^+$	$13/2^+$	1037.8
246.6(3)	2.6(1)	1.25(11)	182/362	$(M1)$	$13/2^-$	$11/2^-$	2313.4
258.3(1)	11.0(3)	0.52(7)	752	$M1$	$19/2^-$	$17/2^-$	2957.7
263.2(4)	2.6(1)				$15/2^-$	$13/2^-$	2576.4
265.4(2)	6.5(2)	0.54(4)	752	$M1$	$25/2^+$	$23/2^+$	3991.7
272.0(2)	2.0(1)	0.58(11)	752	$E1$	$25/2^+$	$23/2^-$	4434.9
286.0(1)	4.7(1)	0.45(15)	752	$M1$	$17/2^-$	$15/2^-$	2699.4
312.1(1)	11.7(4)	1.07(3)	182/362	$M1$	$15/2^-$	$13/2^-$	2413.7
340.5(5)	1.7(1)	1.17(12)	182/362	$(M1)$	$15/2^-$	$13/2^-$	2413.7
348.4(4)	1.8(1)	1.11(15)	182/362	$M1$	$13/2^-$	$11/2^-$	2101.8
352.6(3)	3.6(1)	0.54(6)	752	$M1$	$29/2^+$	$27/2^+$	5315.6
358.7(4)	4.8(2)	1.04(26)	752	$M1/E2$	$17/2^-$	$15/2^-$	2772.5
362.4(1)	35.3(11)	0.55(3)	752	$M1$	$19/2^-$	$17/2^-$	2957.7
366.0(3)	3.4(1)				$9/2^-$	$7/2^-$	1102.5
387.0(4)	1.0(1)				$37/2^-$	$(35/2^-)$	8420.0
396.9(4)	3.6(1)	0.64(9)	752	$M1$	$23/2^+$	$21/2^+$	3726.2
400.3(4)	1.4(1)	0.60(10)	752	$M1$	$23/2^-$	$21/2^-$	4163.7
405.1(1)	22.4(1)	0.51(3)	752	$M1$	$21/2^-$	$19/2^-$	3362.6
420.3(6)	0.7(1)					$17/2^-$	3016.1
425.4(4)	2.4(1)				$(17/2)^+$	$17/2^+$	2316.2
437.0(4)	0.6(1)	0.46(11)	752	$(E1)$	$21/2^-$	$21/2^+$	3764.4
443.0(4)	0.7(1)	0.9(4)	752	$(M1)$	$25/2^+$	$25/2^+$	4434.9
451.1(3)	3.9(1)	0.49(6)	752	$M1$	$29/2^+$	$27/2^+$	5666.5
458.4(5)	0.8(1)				$35/2^-$	$33/2^-$	7906.5
470.5(4)	1.8(1)	1.07(13)	752	$(M1)$	$21/2^+$	$21/2^+$	3329.3
471.0(4)	1.4(1)				$15/2^-$	$15/2^+$	2413.7
483.5(1)	4.2(1)	0.39(8)	752	$M1$	$23/2^-$	$21/2^-$	4083.6
502.9(8)	3.1(1)	0.49(5)	752	$M1$	$27/2^+$	$25/2^+$	4963.1
513.6(8)	2.7(1)	1.10(26)	182/362	$M1$	$37/2^-$	$35/2^-$	8420.0
513.7(5)	1.8(1)				$33/2^-$	$31/2^-$	7447.9
520.0(4)	1.0(1)				$29/2^-$	$27/2^-$	5869.6
522.5(4)	2.6(1)				$29/2^-$	$27/2^-$	5970.1
528.2(4)	1.6(1)	0.47(23)	752	$M1$	$27/2^+$	$25/2^+$	4963.1
533.6(8)	1.6(1)	1.12(30)	182/362	$M1$	$23/2^-$	$21/2^-$	4134.5
542.3(8)	0.7(1)				$21/2^+$	$(17/2^+)$	2859.1
543.4(8)	1.4(1)				$21/2^-$		3559.3
557.4(4)	6.9(2)	0.70(11)	752	$M1/E2$	$25/2^-$	$23/2^-$	4641.3
559.8(2)	7.2(2)				$13/2^-$	$11/2^-$	2313.4
576.8(5)	1.2(1)				$23/2^-$	$21/2^-$	4134.5
576.9(4)	2.4(1)	1.31(25)	182/362	$M1$	$37/2^-$	$35/2^-$	8670.0
577.3(4)	1.0(1)	0.70(13)	752	$M1/E2$	$31/2^-$	$29/2^-$	6934.3
585.3(5)	1.0(1)				$(35/2)^-$	$33/2^-$	8033.1
597.3(5)	5.2(2)				$19/2^-$	$17/2^-$	3194.3
601.3(2)	18.1(6)	0.45(24)	752	$M1$	$21/2^-$	$19/2^-$	3559.3

TABLE I. (*Continued.*)

E_γ^a (keV)	I_γ^b	R_{DCO}^c	$E_\gamma^{\text{GATE } d}$ (keV)	$\sigma\lambda^e$	$J_i^{\pi f}$	$J_f^{\pi g}$	E_i^h (keV)
606.2(5)	3.4(1)				25/2 ⁻	23/2 ⁻	4687.2
643.3(3)	9.9(3)	0.38(7)	752	<i>M1</i>	21/2 ⁻	19/2 ⁻	3600.6
651.2(5)	3.9(1)				11/2 ⁻	9/2 ⁻	1753.6
653.2(2)	13.6(4)	0.58(4)	752	<i>E1</i>	17/2 ⁻	15/2 ⁺	2595.9
660.2(3)	4.2(1)	2.06(13)	182/362	<i>E2</i>	15/2 ⁻	11/2 ⁻	2413.7
663.3(5)	1.5(1)				21/2 ⁻	17/2 ⁻	3362.6
663.3(5)	0.6(1)				27/2 ⁻	25/2 ⁻	5349.6
668.0(5)	2.8(1)	1.82(38)	182/362	<i>E2</i>	21/2 ⁻	17/2 ⁻	3440.6
669.0(6)	0.9(1)				(39/2) ⁻	(37/2) ⁻	9339.0
684.2(5)	2.4(1)				(33/2) ⁻	(31/2) ⁻	7371.6
688.4(8)	1.6(1)				(31/2) ⁻	29/2 ⁻	6557.4
697.1(5)	1.5(1)	0.46(9)	752	<i>M1</i>	33/2 ⁺	31/2 ⁺	7167.0
703.2(3)	4.6(1)	0.53(8)	752	<i>M1</i>	29/2 ⁺	27/2 ⁺	5666.5
707.6(6)	1.1(1)				27/2 ⁻	25/2 ⁻	5349.6
708.5(2)	14.5(4)	0.41(3)	752	<i>M1</i>	25/2 ⁺	23/2 ⁺	4434.9
717.2(3)	5.2(2)				(31/2) ⁻	29/2 ⁻	6687.3
721.0(5)	2.2(1)				(35/2) ⁻	(33/2) ⁻	8093.0
721.5(2)	8.5(3)	0.43(16)	752	<i>M1</i>	23/2 ⁻	21/2 ⁻	4083.6
729.2(6)	2.1(1)				33/2 ⁺	31/2 ⁺	7167.0
731.8(4)	10.0(10)				7/2 ⁻	5/2 ⁻	737.0
734.0(6)	7.1(2)	0.87(14)	752	<i>M1/E2</i>	25/2 ⁺	23/2 ⁺	4460.1
737.0(2)	28.7(9)				7/2 ⁻	5/2 ⁻	737.0
741.1(5)	1.9(1)				21/2 ⁻	17/2 ⁻	3440.6
751.7(1)	100.0(2)				13/2 ⁺	9/2 ⁺	793.5
756.3(4)	2.3(1)				27/2 ⁺	25/2 ⁺	5215.5
771.4(4)	5.0(4)	0.79(14)	752	<i>M1/E2</i>	31/2 ⁺	29/2 ⁺	6437.9
771.9(4)	2.0(2)				23/2 ⁻	21/2 ⁻	4134.5
780.5(5)	7.3(2)				27/2 ⁺	25/2 ⁺	5215.5
786.6(6)	0.7(1)				21/2 ⁻	17/2 ⁻	3559.3
803.4(4)	3.3(2)				31/2 ⁺	29/2 ⁺	6469.9
806.3(3)	2.9(1)	0.67(13)	182/362	(<i>M1</i>)	27/2 ⁻	25/2 ⁻	5447.6
822.6(5)	5.8(2)				15/2 ⁻	11/2 ⁻	2576.4
834.0(5)	2.5(1)				23/2 ⁻	21/2 ⁺	4163.7
838.1(3)	4.7(2)	1.38(37)	182/362	(<i>M1</i>)	35/2 ⁻	33/2 ⁻	7906.5
844.5(2)	14.8(5)	1.28(10)	182/362	<i>E2</i>	21/2 ⁻	17/2 ⁻	3440.6
867.0(2)	29.3(9)	0.45(2)	752	<i>M1</i>	23/2 ⁺	21/2 ⁺	3726.2
890.0(4)	1.7(1)				33/2 ⁻	(31/2) ⁻	7447.9
904.8(3)	3.2(1)				15/2 ⁺	11/2 ⁺	1942.7
935.0(2)	1.2(1)					25/2 ⁻	5576.6
939.4(2)	3.9(1)	1.16(25)	752	<i>E2</i>	23/2 ⁻	19/2 ⁻	4134.5
965.8(5)	2.4(1)				11/2 ⁻	9/2 ⁻	2067.2
969.8(5)	5.9(2)				23/2 ⁻	19/2 ⁻	4163.7
969.9(5)	58.6(18)	0.97(4)	752	<i>E2</i>	21/2 ⁺	17/2 ⁺	2859.1
971.1(2)	8.2(3)				27/2 ⁺	25/2 ⁺	4963.1
995.2(3)	9.5(4)				11/2 ⁺	9/2 ⁺	1037.8
998.9(3)	14.8(5)				13/2 ⁻	9/2 ⁻	2101.8
1011.2(5)	2.0(1)				21/2 ⁺	(17/2) ⁺	3329.3
1016.4(3)	16.5(5)	1.27(8)	182/362	<i>E2</i>	11/2 ⁻	7/2 ⁻	1753.6
1026.8(5)	1.2(1)				35/2 ⁺	33/2 ⁺	8193.3
1033.7(6)	1.3(1)					27/2 ⁺	6249.2
1036.0(6)	2.3(1)				13/2 ⁻	11/2 ⁺	2073.4
1058.7(6)	1.5(1)					25/2 ⁺	5050.4
1082.7(4)	2.1(1)				25/2 ⁻	21/2 ⁻	4641.3
1095.5(1)	87.8(27)	1.08(4)	752	<i>E2</i>	17/2 ⁺	13/2 ⁺	1889.3

TABLE I. (*Continued.*)

E_γ^a (keV)	I_γ^b	R_{DCCO}^c	$E_\gamma^{\text{GATE } d}$ (keV)	$\sigma\lambda^e$	$J_i^{\pi f}$	$J_f^{\pi g}$	E_i^h (keV)
1102.4(2)	18.3(6)	1.73(7)	182/362	$E2$	$9/2^-$	$5/2^-$	1102.5
1104.5(5)	3.6(1)				$25/2^+$	$21/2^+$	4434.9
1126.9(1)	8.0(2)	2.06(14)	182/362	$E2$	$25/2^-$	$21/2^-$	4687.2
1132.4(1)	21.1(6)	1.1(5)	752	$E2$	$25/2^+$	$21/2^+$	3991.7
1142.4(3)	2.7(1)					$25/2^+$	5576.6
1149.0(1)	19.3(6)	0.31(2)	752	$M1$	$15/2^+$	$13/2^+$	1942.7
1168.5(3)	1.7(1)				$15/2^+$	$11/2^+$	2206.1
1178.1(5)	0.5(1)						4714.6
1182.7(2)	9.4(3)	2.38(18)	182/362	$E2$	$29/2^-$	$25/2^-$	5869.6
1198.8(3)	8.5(3)	2.61(29)	182/362	$E2$	$33/2^-$	$29/2^-$	7068.4
1207.1(6)	1.5(1)					$27/2^+$	6422.6
1207.3(5)	4.7(15)				$(31/2)^-$	$27/2^-$	6557.4
1210.5(3)	6.9(22)	1.82(13)	182/362	$E2$	$13/2^-$	$9/2^-$	2313.4
1214.8(3)	6.6(21)	2.16(64)	182/362	$E2$	$27/2^-$	$23/2^-$	6422.6
1218.6(5)	1.8(1)					$(17/2)^+$	3535.2
1223.5(5)	1.3(1)				$27/2^+$	$25/2^+$	5215.5
1232.0(6)	4.6(14)				$29/2^+$	$25/2^+$	5666.5
1239.5(7)	0.4(1)				$(31/2)^-$	$27/2^-$	6687.3
1246.2(2)	9.0(3)	1.14(17)	752	$E2$	$25/2^-$	$21/2^-$	4687.2
1247.1(4)	0.2(1)				$(39/2)^-$	$35/2^-$	9339.0
1269.9(3)	1.3(1)					$21/2^+$	4129.1
1275.6(5)	3.0(1)				$13/2^-$	$11/2^+$	2313.4
1278.8(2)	6.0(2)	1.78(12)	182/362	$E2$	$25/2^-$	$21/2^-$	4641.3
1300.4(5)	0.5(1)				$(37/2)^-$	$(33/2)^-$	8670.0
1305.2(3)	7.6(2)	0.58(8)	752	$E1$	$19/2^-$	$17/2^+$	3194.3
1323.8(3)	9.5(3)				$29/2^+$	$25/2^+$	5315.6
1328.7(3)	5.1(2)	1.84(15)	182/362	$E2$	$29/2^-$	$25/2^-$	5970.1
1349.5(4)	2.0(1)				$35/2^-$	$31/2^-$	7906.5
1351.3(5)	2.9(1)	0.91(16)	752	$E2$	$37/2^-$	$33/2^-$	8420.0
1351.9(6)	0.9(1)					$29/2^+$	6668.6
1363.0(5)	0.5(1)				$27/2^-$	$23/2^-$	5447.6
1372.8(5)	1.4(1)					$25/2^+$	6087.4
1385.5(4)	3.3(1)					$21/2^+$	4714.6
1402.1(7)	1.2(1)				$(33/2)^-$	$29/2^-$	7371.6
1406.5(6)	0.6(1)				$(35/2)^-$	$(31/2)^-$	8093.0
1440.5(2)	10.7(3)	1.19(11)	752	$E2$	$21/2^+$	$17/2^+$	3329.3
1448.2(5)	0.7(1)				$21/2^-$	$17/2^+$	3764.4
1474.3(4)	1.5(1)				$31/2^+$	$27/2^+$	6437.9
1476.0(5)	0.7(1)				$(35/2)^-$	$(31/2)^-$	8033.1
1490.7(4)	1.7(1)	2.1(4)	182/362	$E2$	$41/2^-$	$37/2^-$	9910.7
1500.7(4)	1.8(1)				$33/2^+$	$29/2^+$	7167.0
1524.7(2)	5.1(2)				$(17/2)^+$	$13/2^+$	2316.2
1545.2(5)	0.6(1)						7632.6
1576.1(6)	1.8(1)				$25/2^+$	$21/2^+$	4434.9
1597.0(4)	5.8(2)				$(33/2)^+$	$29/2^+$	6912.7
1601.0(6)	0.6(1)				$(39/2)^-$	$(35/2)^-$	9634.1
1602.9(4)	2.2(1)				$25/2^+$	$21/2^+$	4460.1
1620.2(2)	10.1(3)	0.77(5)	752	$E1$	$15/2^-$	$13/2^+$	2413.7
1670.4(5)	0.8(1)				$29/2^-$	$25/2^-$	6357.2
1696.0(7)	0.9(1)					$27/2^+$	6911.5
1706.0(6)	1.6(1)					$27/2^+$	6668.6
1754.3(6)	0.9(1)				$(35/2)^+$	$31/2^+$	8193.3
1804.6(7)	0.6(1)				$(45/2)^-$	$41/2^-$	11715.3
1924.4(6)	1.2(1)				$(37/2)^+$	$(33/2)^+$	8837.0
2025.1(6)	0.9(1)				$11/2^-$	$9/2^+$	2067.2

TABLE I. (*Continued.*)

E_γ^a (keV)	I_γ^b	R_{DCO}^c	$E_\gamma^{\text{GATE } d}$ (keV)	$\sigma\lambda^e$	$J_i^{\pi f}$	$J_f^{\pi g}$	E_i^h (keV)
2049.3(8)	0.6(1)					(33/2) ⁺	8961.9
2211.4(8)	0.2(1)				(49/2) ⁻	(45/2) ⁻	13926.7

^aTransition energy. The error in units of the last digit is given in parentheses.

^bRelative intensity of the γ ray normalized to $I_\gamma = 100$ of the $17/2_1^+ \rightarrow 9/2_1^+$ transition at 751.7 keV.

^cDCO ratio $R_{\text{DCO}} = W(90^\circ, 35^\circ/145^\circ)/W(35^\circ/145^\circ, 90^\circ)$.

^dEnergy of the gating transition used for the determination of the DCO ratio.

^eMultipolarity compatible with the DCO ratio and the de-excitation mode.

^fSpin and parity of the initial state.

^gSpin and parity of the final state.

^hEnergy of the initial state.

E_γ - E_γ matrices containing coincidence events of all detector pairs including one detector at 35° or 145° , respectively. The lifetimes were deduced from a comparison of experimental with calculated line shapes. The velocity distributions of the emitting nuclei were calculated with a Monte Carlo code taking into account reactions at different depths in the target, the kinematics of the reaction, and the slowing-down and straggling of the recoil nuclei [46]. For the slowing-down the cross sections given in Ref. [47] were used with correction factors of $f_e = 0.9$ and $f_n = 0.7$ for the electronic and nuclear stopping powers, respectively [8,13,33,48–50]. To extract the level lifetimes, cascade feeding from all levels observed above the considered one as well as sidefeeding from unobserved levels was taken into account. The sidefeeding time was assumed to be zero for the excitation energy $E^* = 11.6$ MeV derived from the relation $E^* = E_{11\text{B}}^{\text{CM}} + Q - N_n \times E_n$, where Q and $N_n \times E_n$ denote the Q value and the mean total energy of the N emitted neutrons, respectively, with values of $Q = -17.8$ MeV and $N_n \times E_n = 10$ MeV. The values of E_n correspond to mean energies of emitted neutrons calculated with evaporation codes as described, e.g., in Ref. [7]. With decreasing excitation energy an increase of the sidefeeding times according to $\tau_{s,f} = (E^* - E/\text{MeV}) \times 0.03$ ps was assumed [8,13,33,48–50]. Examples of the line-shape analysis are shown in Fig. 2. The two calculated line shapes corresponding to the complementary observation angles of 35° and 145° were optimized simultaneously in one least-squares fit. This allowed background peaks to be taken into account correctly (cf. Fig. 2). For a given transition, several fits were carried out in which the feeding times and feeding intensities were varied within their errors. In this way the influence of these quantities on the lifetimes and, thus, the uncertainties of the lifetimes because of the errors of feeding times and feeding intensities were determined.

The lifetimes obtained from this analysis are given in Table II. The present lifetimes of the levels at 1889.3 and 2859.1 keV are not consistent with the considerably smaller values deduced in Ref. [36] but agree within their uncertainties with the values from earlier work [51] given for comparison in Ref. [36]. The lifetime of the 3991.7-keV level quoted in Ref. [36] is also considerably smaller than the present value, whereas the upper limit given for the lifetime of

TABLE II. Mean lifetimes of states in ^{83}Rb .

E_i (keV) ^a	E_γ (keV) ^b	τ (ps) ^c
$\pi = +$		
1889	1095.5	1.55(18)
2316	1524.7	< 5 ^d
2859	969.9	2.03(19)
3329	1440.5	< 1.3 ^d
3726	867.0	0.23(4)
3992	1132.4	0.96(9)
4435	708.5	0.45(14)
4460	734.0	0.42(12)
5316	1323.8	0.34(5)
6913	1597.0	0.18(2)
$\pi = -$		
3194	1305.2	< 1.3 ^d
3601	643.3	0.41(8)
4084	483.5	0.33(3)
4641	557.4/1278.8	0.39(5)
4687	1246.2	0.48(6)
5448	806.3	0.05(2)
5870	1182.7	0.56(8)
5970	522.5/1328.7	0.45(5)
6687	717.2	0.16(3)
7068	1198.8	0.27(9)
7372	1402.1	0.09(3)
8093	1406.5	0.24(8)
8670	576.9	0.24(4) ^e

^aLevel energy.

^bEnergy of the γ ray used for the line-shape analysis in connection with the DSA method.

^cAdopted level lifetime. The error in parentheses includes the statistical error, uncertainties of feeding times, feeding intensities, and a 5% uncertainty of the nuclear and electronic stopping power.

^dUpper limit deduced from the effective lifetime without feeding correction.

^eThe line shape of the 576.9-keV transition was analysed in a spectrum gated on the 483.5- and 643.3-keV transitions and may be influenced by small contributions from the 577.3-keV transition linking the states at 6357.2 and 6934.3 keV.

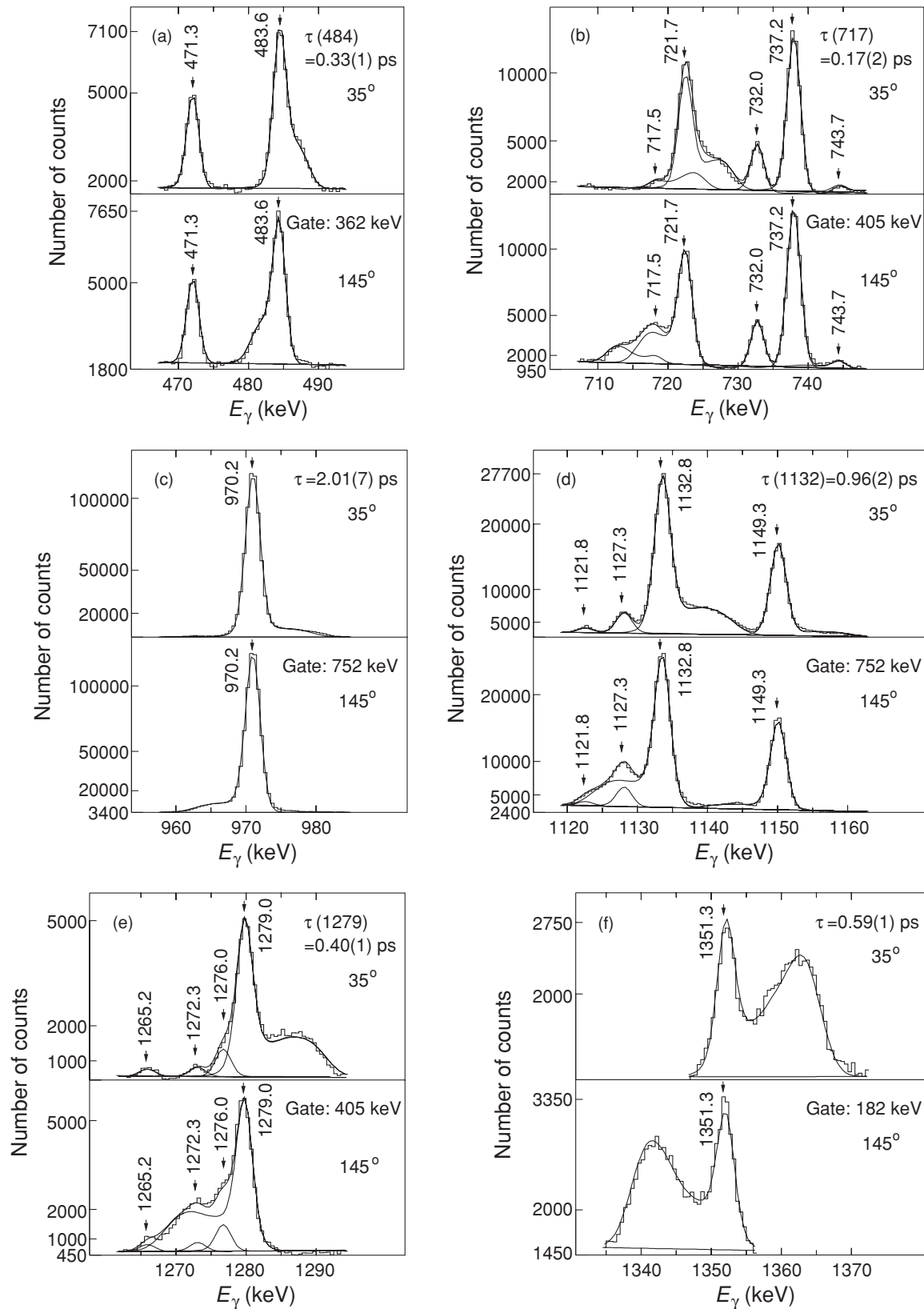


FIG. 2. Examples of the line-shape analysis using the DSA method. The lifetimes were deduced from simultaneous fits of calculated to experimental line shapes at the complementary observation angles of 35° and 145° . Feeding corrections are included. The given values of energies, lifetimes and their errors are results of the presented individual fits. In case of multiplets the lifetimes refer to the transition energies in parentheses.

TABLE III. Experimental and calculated transition strengths in ^{83}Rb .

E_γ (keV)	J_i^π	J_f^π	$\sigma\lambda$	$B(\sigma\lambda)_{\text{EXP}}^a$	$B(\sigma\lambda)_{\text{SM}}^a$
1095.5	$17/2_1^+$	$13/2_1^+$	$E2$	334_{-34}^{+44}	455
1524.7	$17/2_2^+$	$13/2_1^+$	$E2$	>12	0.02
425.4	$17/2_2^+$	$17/2_1^+$	$M1$	>43	81
969.9	$21/2_1^+$	$17/2_1^+$	$E2$	464_{-41}^{+49}	414
542.3	$21/2_1^+$	$17/2_2^+$	$E2$	101_{-24}^{+30}	29
1440.5	$21/2_2^+$	$17/2_1^+$	$E2$	>73	4.1
1011.2	$21/2_2^+$	$17/2_2^+$	$E2$	>76	88
470.5	$21/2_2^+$	$21/2_1^+$	$M1$	>48	90
867.0	$23/2_1^+$	$21/2_1^+$	$M1$	335_{-51}^{+73}	1110
396.9	$23/2_1^+$	$21/2_2^+$	$M1$	428_{-82}^{+117}	418
1132.4	$25/2_1^+$	$21/2_1^+$	$E2$	350_{-34}^{+41}	393
265.4	$25/2_1^+$	$23/2_1^+$	$M1$	739_{-94}^{+113}	1170
1576.1	$25/2_2^+$	$21/2_1^+$	$E2$	15_{-4}^{+8}	95
1104.5	$25/2_2^+$	$21/2_2^+$	$E2$	176_{-49}^{+94}	47
708.5	$25/2_2^+$	$23/2_1^+$	$M1$	226_{-58}^{+110}	166
272.0	$25/2_2^+$	$23/2_3^-$	$E1$	6_{-2}^{+3}	–
443.0	$25/2_2^+$	$25/2_1^+$	$M1$	45_{-16}^{+31}	0.46
1602.9	$25/2_3^+$	$21/2_1^+$	$E2$	44_{-12}^{+20}	0.01
734.0	$25/2_3^+$	$23/2_1^+$	$M1$	259_{-61}^{+109}	0.02
1323.8	$29/2_1^+$	$25/2_1^+$	$E2$	429_{-61}^{+82}	411
352.6	$29/2_1^+$	$27/2_1^+$	$M1$	1038_{-172}^{+231}	1400
1597.0	$33/2_1^+$	$29/2_1^+$	$E2$	437_{-44}^{+54}	390
181.9	$17/2_1^-$	$15/2_1^-$	$M1$	3383 ± 1002^b	44
362.4	$19/2_1^-$	$17/2_1^-$	$M1$	895_{-251}^{+286b}	102
1305.2	$19/2_2^-$	$17/2_1^+$	$E1$	>190	–
237.2	$19/2_2^-$	$19/2_1^-$	$M1$	>335	29
601.3	$21/2_3^-$	$19/2_1^-$	$M1$	609_{-215}^{+465b}	32
643.3	$21/2_4^-$	$19/2_1^-$	$M1$	448_{-78}^{+115}	4
238.1	$21/2_4^-$	$21/2_1^-$	$M1$	1338_{-312}^{+465}	18
721.5	$23/2_1^-$	$21/2_1^-$	$M1$	304_{-31}^{+37}	22
483.5	$23/2_1^-$	$21/2_4^-$	$M1$	499_{-60}^{+72}	1
1278.8	$25/2_1^-$	$21/2_1^-$	$E2$	245_{-37}^{+47}	360
1082.7	$25/2_1^-$	$21/2_3^-$	$E2$	197_{-34}^{+44}	0.005
557.4	$25/2_1^-$	$23/2_1^-$	$M1$	383_{-56}^{+72}	296
1246.2	$25/2_2^-$	$21/2_2^-$	$E2$	250_{-35}^{+45}	31
1126.9	$25/2_2^-$	$21/2_3^-$	$E2$	368_{-52}^{+67}	37
606.2	$25/2_2^-$	$23/2_1^-$	$M1$	88_{-14}^{+17}	4
1363.0	$27/2_2^-$	$23/2_1^-$	$E2$	511_{-219}^{+511}	206
806.3	$27/2_2^-$	$25/2_1^-$	$M1$	1832_{-78}^{+1326}	36
1182.7	$29/2_1^-$	$25/2_2^-$	$E2$	570_{-103}^{+103}	38
520.0	$29/2_1^-$	$27/2_1^-$	$M1$	69_{-16}^{+21}	10
1328.7	$29/2_2^-$	$25/2_1^-$	$E2$	291_{-36}^{+45}	0.6
522.5	$29/2_2^-$	$27/2_2^-$	$M1$	296_{-43}^{+54}	0.0002
1239.5	$31/2_2^-$	$27/2_2^-$	$E2$	125_{-48}^{+70}	0.3
717.2	$31/2_2^-$	$29/2_2^-$	$M1$	886_{-155}^{+226}	518
1198.8	$33/2_1^-$	$29/2_1^-$	$E2$	1223_{-611}^{+1326}	187
1402.1	$33/2_2^-$	$29/2_2^-$	$E2$	559_{-174}^{+349}	266

TABLE III. (*Continued.*)

E_γ (keV)	J_i^π	J_f^π	$\sigma\lambda$	$B(\sigma\lambda)_{\text{EXP}}^a$	$B(\sigma\lambda)_{\text{SM}}^a$
684.2	$33/2_2^-$	$31/2_2^-$	$M1$	1302_{-366}^{+732}	1510
1406.5	$35/2_3^-$	$31/2_2^-$	$E2$	133_{-50}^{+99}	12
721.0	$35/2_3^-$	$33/2_2^-$	$M1$	492_{-140}^{+279}	7
1300.4	$37/2_2^-$	$33/2_2^-$	$E2$	158_{-50}^{+70}	0.06
576.9	$37/2_2^-$	$35/2_3^-$	$M1$	1011_{-181}^{+253}	651

^aReduced transition strengths: $B(M1)$ in $10^{-3} \mu_N^2$; $B(E1)$ in $10^{-6} e^2 \text{fm}^2$; $B(E2)$ in $e^2 \text{fm}^4$. Weisskopf units: 1 W.u.($M1$) = 1.79 μ_N^2 ; 1 W.u.($E1$) = 1.23 $e^2 \text{fm}^2$; 1 W.u.($E2$) = 21.51 $e^2 \text{fm}^4$.

^bValue taken from Ref. [36].

the 5315.6-keV level in Ref. [36] is compatible with the value deduced from the present analysis. Transition strengths deduced from the present lifetimes are listed in Table III.

III. LEVEL SCHEME

The level scheme of ^{83}Rb as established from γ - γ and γ - γ - γ coincidence relations and γ -ray intensities in the present thin-target experiment [12,38,39] is shown in Fig. 3. Spin and parity assignments are based on DCO ratios of the γ rays as well as on de-excitation modes and lifetimes. Multipolarity $M2$ has been excluded for quadrupole transitions, because the usual $M2$ transition strengths known in this mass region [52] correspond to lifetimes of $\tau = 100$ ns or more. The lifetimes in the ps region determined in the present work (see Table II) exclude multipolarity $E1$ for dipole transitions, because the resulting $E1$ transition strengths would exceed those known in this mass region [52] by about two orders of magnitude. Whenever spin and parity assignments for low-lying states were not possible on the basis of the present data, we adopted the assignments known from previous work [34–36].

Positive-parity states have been known from Refs. [35,36] up to a $(37/2^+)$ state at 8834 keV and were confirmed in the present study. We found additional levels at 6437.9, 6469.9, 7167.0, and 8193.3 keV and grouped them into a $\Delta J = 1$ level sequence (sequence A in Fig. 3).

The negative-parity states given in Refs. [34,36] have been confirmed in the present work. Several additional transitions linking low-lying states have been observed. The spin assignments of $13/2^-$, $15/2^-$, $17/2^-$, $19/2^-$, and $21/2^-$ made on the basis of the present DCO ratios for the levels at 2313.4, 2413.7, 2595.9, 2957.7, and 3362.6 keV, respectively, are in agreement with those given in Refs. [34,36]. On top of the 3362.6-keV level we observed a sequence of $E2$ transitions (sequence B in Fig. 3). We established another $E2$ sequence starting on top of a $17/2^-$ state at 2772.5 keV (sequence C in Fig. 3) that may be considered as the signature partner of sequence B. This sequence C was observed in Ref. [36] up to the $33/2^-$ state at 7068.4 keV and was extended in the present work up to the $(49/2)^-$ state. We observed a sequence of levels at 6357.2, 6934.3, 7447.9, and 7906.5 keV, which are connected with levels of both sequences B and C. Furthermore,

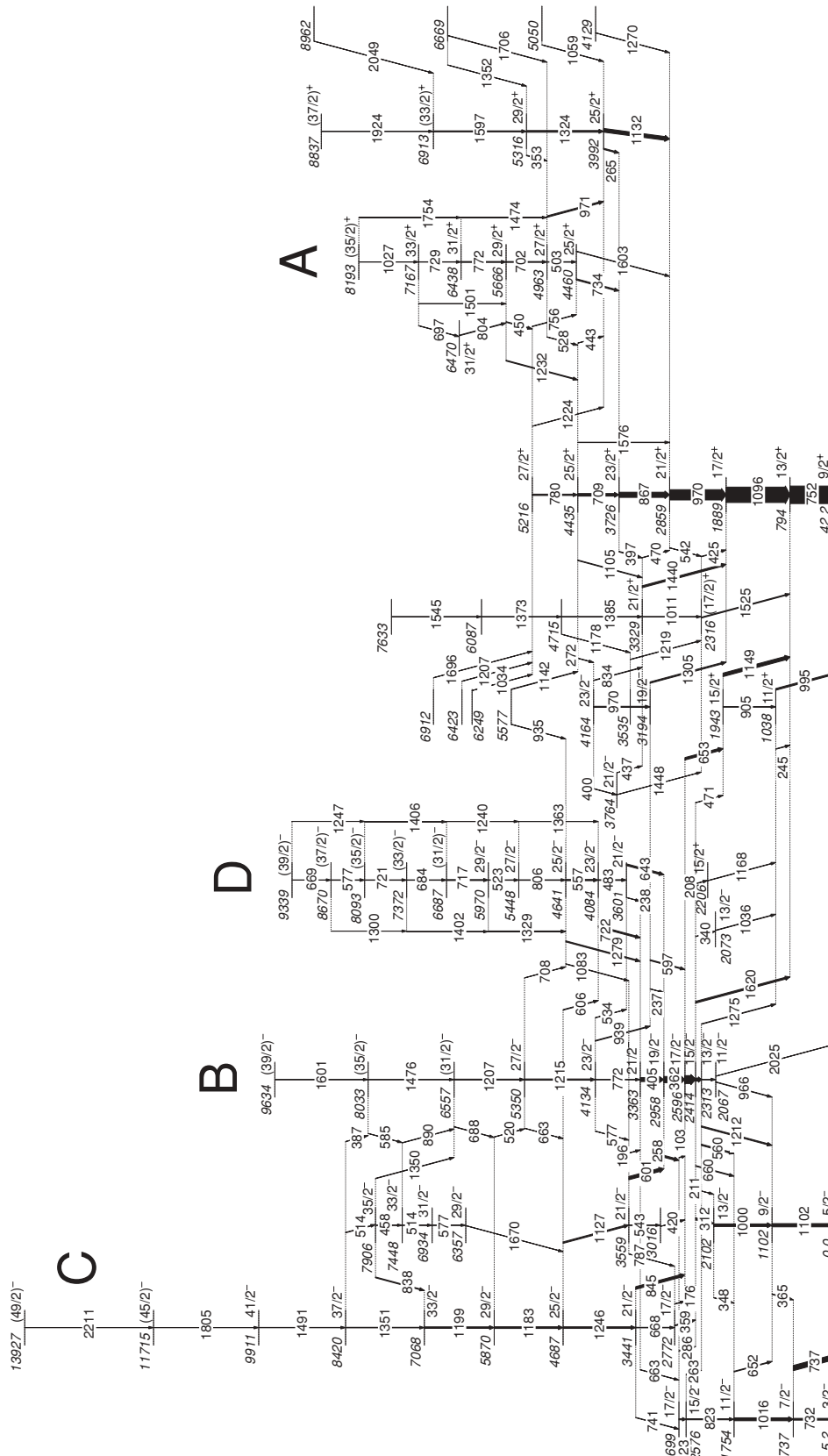


FIG. 3. Level scheme of ⁸³Rb deduced from the present experiments.

we established a $\Delta J = 1$ level sequence, including dipole as well as crossover quadrupole transitions (sequence D in Fig. 3), which is linked with known low-lying levels as well as with levels of sequences B and C. The lowest states of sequence D up to the $27/2^-$ state at 5448.4 keV were also observed in Ref. [36], whereas in the present work this sequence was extended up to the $(39/2)^-$ state.

In addition to the discussed structures, several transitions connecting low-lying states were newly identified.

IV. INTERPRETATION

In the irregular sequence A the branches with signatures $\alpha = +1/2$ and $\alpha = -1/2$ are linked by $M1$ transitions of relatively large energies. Note that the states of the $\alpha = -1/2$ branch starting with $J^\pi = 27/2^+$ are yrast states, whereas the states of the $\alpha = +1/2$ branch are not yrast. The $\alpha = +1/2$ yrast states form a separate sequence connected by $E2$ transitions instead. The $E2$ sequence B is built on top of the sequence of four intense $M1$ transitions at 100.1, 181.9, 362.4, and 405.1 keV. This change from an $M1$ sequence to an $E2$ sequence indicates a change of the configuration. Sequence B includes an irregularity as indicated by the nearly equal level spacings between the $23/2^-$, $27/2^-$, and $31/2^-$ states. The $E2$ sequence C includes an irregularity shown by the nearly equal level spacings between the $25/2^-$, $29/2^-$, and $33/2^-$ states. The reduced $E2$ transition strengths given in Table III indicate little collectivity for the $21/2^-$ and $25/2^-$ states of sequence C but an increase of collectivity for the higher-lying states of this sequence.

The $M1$ sequence D resembles at a first glance the negative-parity $M1$ bands found in the neighboring odd-odd isotopes ^{82}Rb and ^{84}Rb [32,33]. A closer inspection, however, shows remarkable differences. Figure 4 displays the spins J and the reduced $M1$ transition strengths, respectively, as a function of the rotational frequency that is equivalent to the energy of an $M1$ transition, $\hbar\omega = E_\gamma(M1)$. The $M1$ bands in ^{82}Rb and ^{84}Rb follow the regular behavior of a rotational band, which means that the spin is a smooth function of the rotational frequency, $J \sim \hbar\omega$. The $B(M1)$ values within these bands decrease with increasing spin or increasing rotational frequency, thus indicating magnetic rotation and the shears mechanism. In contrast to these characteristics, sequence D in ^{83}Rb shows an irregular, multiplet-like behavior of J as a function of $\hbar\omega$, and the $B(M1)$ values do not follow the pattern of the shears mechanism, i.e., they do not decrease continuously with increasing rotational frequency. The positive-parity $M1$ sequence A is also not regular. These striking differences between the $M1$ sequences in ^{83}Rb and those in the neighboring isotopes ^{82}Rb and ^{84}Rb must have their origin in the neutron numbers, which are odd in ^{82}Rb and ^{84}Rb and even in ^{83}Rb . The isotopes $^{82}\text{Rb}_{45}$ and $^{84}\text{Rb}_{47}$ have an unpaired proton as well as an unpaired neutron. Breaking one pair of nucleons results in a four-quasiparticle (4qp) configuration. In fact, the configuration $\pi(fp)\pi(g_{9/2}^2)\nu(g_{9/2})$ was ascribed to the negative-parity $M1$ sequences in ^{82}Rb and ^{84}Rb [32,33]. The isotope $^{83}\text{Rb}_{46}$ has an unpaired proton only. Breaking one pair of nucleons results in a 3qp

configuration. In earlier work [34,37] the configuration $\pi(g_{9/2})\nu(g_{9/2})\nu(fp)$ was proposed for the sequence of intense $M1$ transitions connecting $13/2^-$ to $21/2^-$ states, which does not correspond to the configuration assigned to the negative-parity $M1$ sequences in ^{82}Rb and ^{84}Rb [32,33]. Instead of lifting protons from the almost completely filled (fp) subshell to the empty $g_{9/2}$ orbits, in the configuration $\pi(g_{9/2})\nu(g_{9/2})\nu(fp)$ a neutron is excited from the (fp) subshell to the $g_{9/2}$ orbit that contains already six neutrons. This configuration is exhausted at $J = 21/2$ or $23/2$, if the neutron is taken from the $p_{3/2}$ or the $f_{5/2}$ orbit, respectively. Indeed, the present work has shown that this $M1$ sequence terminates at $21/2^-$ and is taken over by the $E2$ sequence B. The $M1$ sequence D probably contains a 5qp configuration that is necessary to generate high spins. In addition, the irregularity of this sequence reveals that the underlying configuration cannot maintain the shears mechanism. An interpretation within the TAC model is consequently not adequate for the $M1$ sequence in ^{83}Rb . Instead, we describe in the following an interpretation in the framework of the spherical shell model. We applied the shell model already to the negative-parity $M1$ band in the neighboring odd-odd isotope ^{84}Rb as an alternative to the interpretation within the TAC model [33]. It turned out that the shell model in the used configuration space was not able to reproduce the regular $M1$ band. In an earlier shell-model study of shears bands in light Pb nuclei it was found that regular bands can be created, if several high- j protons and high- j neutron holes interact with many low-spin orbitals [53,54]. If one applies this to ^{83}Rb or ^{84}Rb , then the number of proton particle-hole excitations of the type $\pi[(0f_{5/2}^{-1}1p_{3/2})^{-m-1}(1p_{1/2}0g_{9/2})^m]$ should be such that the number of particles in the fp shell is in the middle of the shell ($m \approx 4$ to 6). However, in the calculations for ^{84}Rb described in Ref. [33] and for ^{83}Rb described in the following this number had to be limited to $m = 3$. Nevertheless, the calculations for ^{84}Rb delivered alternative information about the configuration involved in the $M1$ band. In fact, the configuration $\pi(0f_{5/2}^{-2}1p_{3/2}^{-1}0g_{9/2}^2)\nu(0g_{9/2}^{-3})$ proposed for the $M1$ band in ^{84}Rb on the basis of the shell-model calculations is consistent with the configuration predicted by the TAC model and reproduces the magnitude of the experimental transition strengths [33]. Therefore, we expect that analogous shell-model calculations deliver information also about configurations and properties of the level sequences in ^{83}Rb , in particular of the irregular $M1$ sequence D.

A. Shell-model calculations

The model space used in our calculations for ^{83}Rb (37 protons and 46 neutrons) includes the active proton orbits $\pi(0f_{5/2}, 1p_{3/2}, 1p_{1/2}, 0g_{9/2})$ and neutron orbits $\nu(1p_{1/2}, 0g_{9/2})$ relative to a hypothetical ^{66}Ni core. Because a complete empirical set of effective interactions for this model space has not been available until now, various empirical interactions have been combined with schematic nuclear interactions applying the surface delta interaction. Details of this procedure are described in our previous shell-model studies of

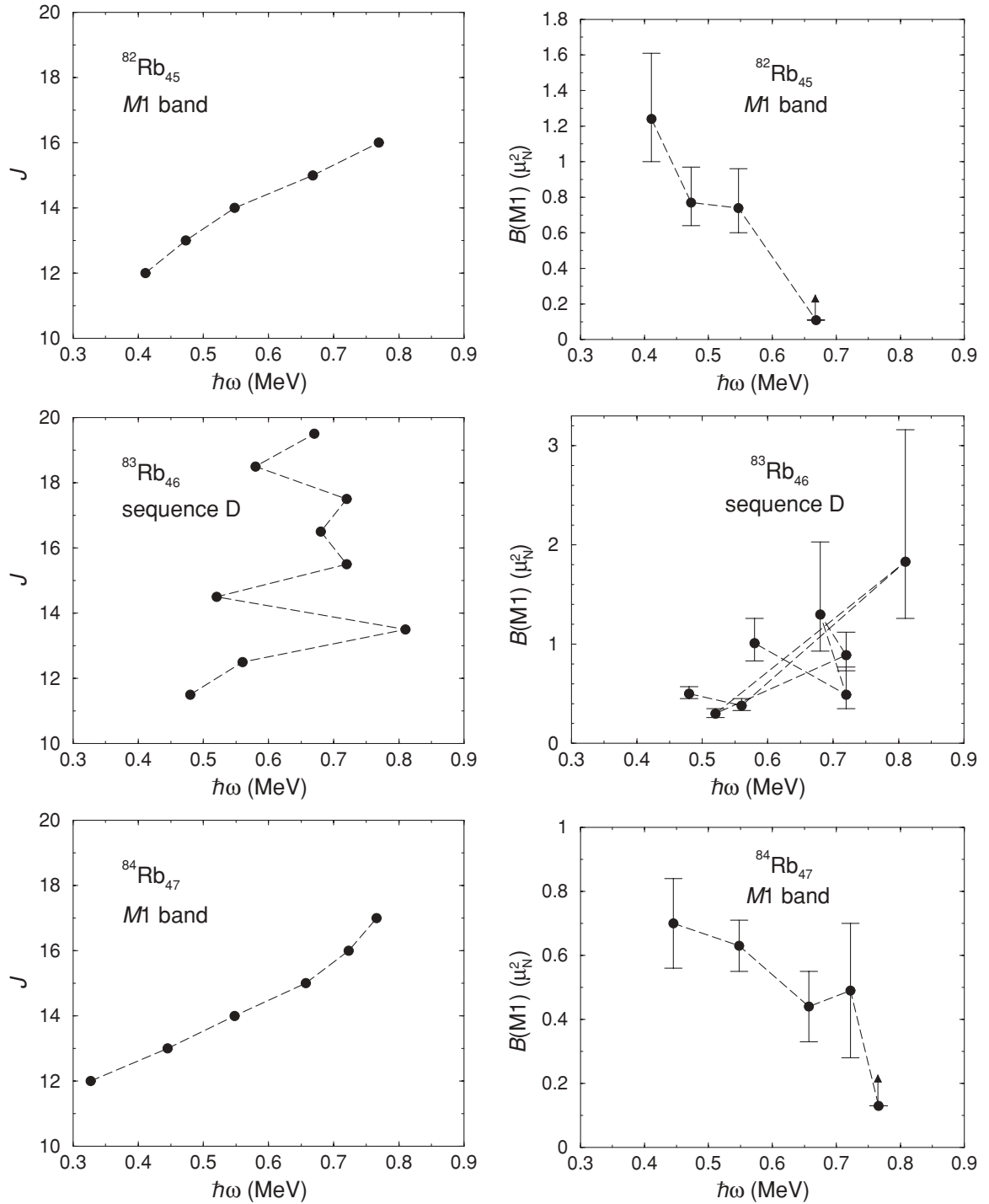


FIG. 4. Spins J and reduced $M1$ transition strengths as functions of the rotational frequency $\hbar\omega$ for the negative-parity $M1$ sequences in ^{82}Rb , ^{83}Rb , and ^{84}Rb . The rotational frequency corresponds to the $M1$ transition energy. The points are connected such that the dashed line follows the level sequence from low to high spin. The data for ^{82}Rb and ^{84}Rb were taken from Ref. [33].

nuclei with $N = 47 - 54$ [13,33,49,50,55–63]. This is the first attempt to apply this model space and set of interactions to an $N = 46$ nuclide. Earlier shell-model calculations for $N = 46$ nuclides were carried out for $Z \geq 40$ only and applied a $\pi(1p_{1/2}, 0g_{9/2})\nu(1p_{1/2}, 0g_{9/2})$ model space relative to an ^{88}Sr core [64,65].

The single-particle energies relative to the ^{66}Ni core have been derived from the single-particle energies of the proton orbits given in Ref. [66] with respect to the ^{78}Ni core and from the neutron single-hole energies of the $1p_{1/2}, 0g_{9/2}$ orbits [67]. The transformation of these single-particle energies to those relative to the ^{66}Ni core [68] has been performed on the

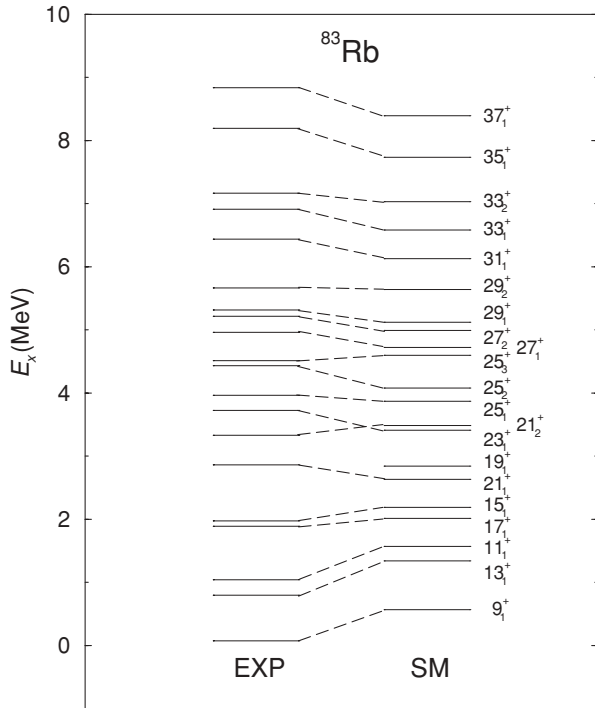


FIG. 5. Comparison of experimental with calculated energies of positive-parity states in ^{83}Rb . Spins are given as $2J$.

basis of the effective residual interactions given in, e.g., Refs. [49,56]. The obtained values are $\epsilon_{f_{5/2}}^\pi = -9.106$ MeV, $\epsilon_{p_{3/2}}^\pi = -9.033$ MeV, $\epsilon_{p_{1/2}}^\pi = -4.715$ MeV, $\epsilon_{g_{9/2}}^\pi = -0.346$ MeV, $\epsilon_{p_{1/2}}^\nu = -7.834$ MeV, and $\epsilon_{g_{9/2}}^\nu = -6.749$ MeV. These single-particle energies and the corresponding values for the strengths of the residual interactions have been used to calculate level energies as well as $M1$ and $E2$ transition strengths. For the latter, effective g factors of $g_s^{\text{eff}} = 0.7g_s^{\text{free}}$ and effective charges of $e_\pi = 1.72e$, $e_\nu = 1.44e$ [69], respectively, have been applied.

The nucleus ^{83}Rb has nine protons and eight neutrons in the considered configuration space. To make the calculations feasible a truncation of the occupation numbers was applied. At most three protons were allowed to be lifted to the $(1p_{1/2}, 0g_{9/2})$ subshell. Two of the neutrons occupy the $1p_{1/2}$ orbit and six the $0g_{9/2}$ orbit. With these restrictions configuration spaces with dimensions up to 32451 at $J^\pi = 13/2^+$ were obtained. We had also tested a configuration space including neutron excitations from the $1p_{1/2}$ orbit to the $0g_{9/2}$ orbit to allow configurations of the type $\pi(g_{9/2})\nu(g_{9/2})\nu(fp)$ as proposed in Refs. [34,37] for the $13/2^-$ to $21/2^-$ states linked by intense $M1$ transitions. It turned out that the contributions of such excitations to the wave functions are negligibly small. Therefore, we limited the occupation numbers in the neutron orbits as described before. The calculations were carried out with the code RITSSCHIL [70].

B. Results for positive-parity states

Experimental and calculated positive-parity states are compared in Fig. 5. The experimental states are in general reproduced by the calculated ones. The calculated states up

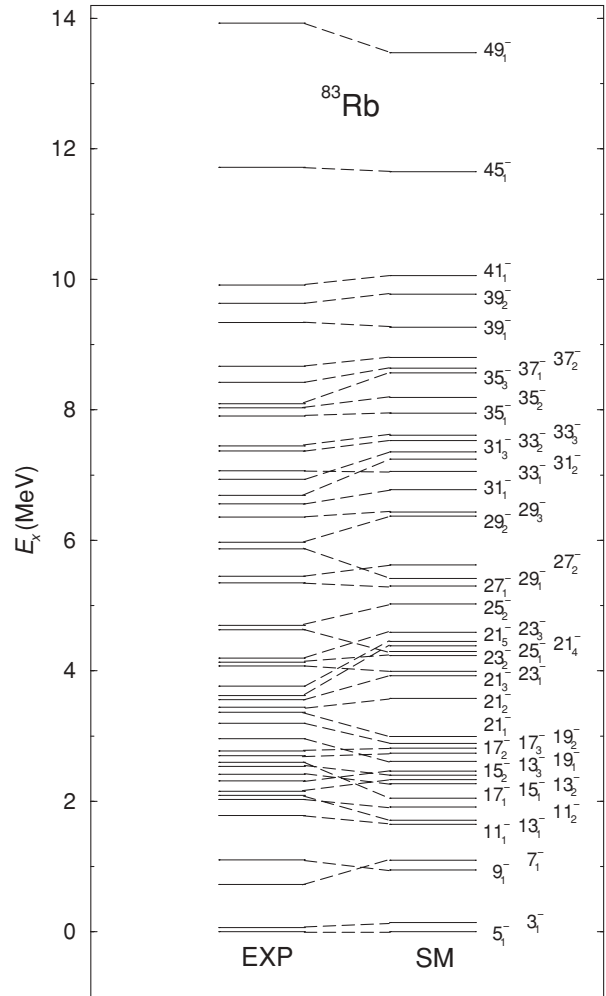


FIG. 6. Comparison of experimental with calculated energies of negative-parity states in ^{83}Rb . Spins are given as $2J$.

to $J^\pi = 13/2^+$ are predicted somewhat too high, whereas the states with $J \geq 31/2$ tend to be below the experimental ones. The $9/2_1^+$ state is mainly the $\pi(0g_{9/2}^1)$ excitation. The $11/2_1^+$ to $25/2_1^+$ states are dominated by the configuration $\pi(0g_{9/2}^1)\nu(0g_{9/2}^{-4})_{J_\nu}$ with neutron spins $J_\nu = 2$ to 8 , whereas at higher spin the two (fp) proton holes are also active, leading to the main configurations $\pi(0f_{5/2}^{-2}0g_{9/2}^1)\nu(0g_{9/2}^{-4})_{J_\nu}$ for the $27/2_1^+$, $29/2_1^+$, $33/2_1^+$, and $37/2_1^+$ states and $\pi(0f_{5/2}^{-1}1p_{3/2}^{-1}0g_{9/2}^1)\nu(0g_{9/2}^{-4})_{J_\nu}$ for the $31/2_1^+$ and $35/2_1^+$ states. At $J = 33/2$ a second $0g_{9/2}$ neutron pair is broken resulting in $J_\nu = 10, 12$ for the states with $J \geq 33/2$. The second and third states of a given spin contain equivalent configurations with varying partitions. Calculated transition strengths are compared with experimental ones in Table III. The calculated values are compatible with the experimental values with the exception of some strengths of transitions from second or third states of a given spin.

C. Results for negative-parity states

Experimental and calculated energies of negative-parity states displayed in Fig. 6 are in a general agreement, although

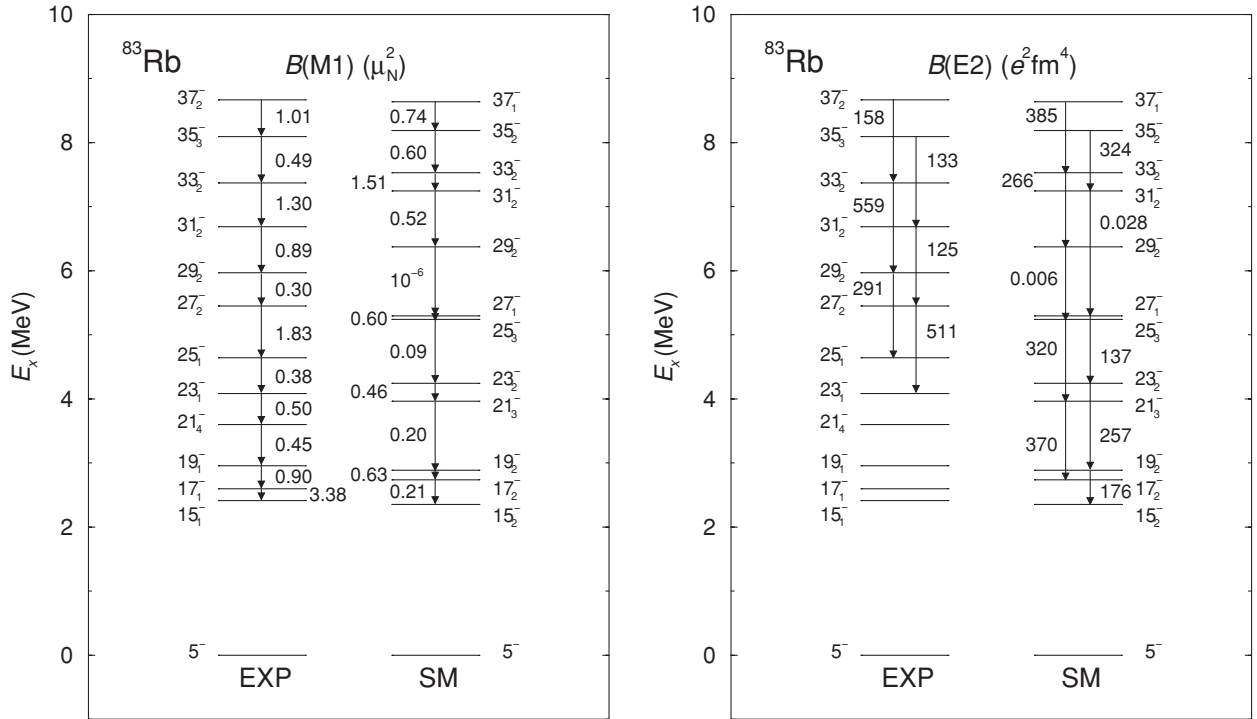


FIG. 7. Comparison of level energies, $B(M1)$, and $B(E2)$ transition strengths of band D with calculated ones. Spins are given as $2J$.

there are differences in level energies and in the order of states especially at low spin. The $3/2_1^-$ and $5/2_1^-$ states are characterized by the $\pi(1p_{3/2}^{-1})$ and $\pi(0f_{5/2}^{-1})$ configurations, respectively. In the $7/2_1^-$ to $29/2_1^-$ states the configuration $\pi(0f_{5/2}^{-1})\nu(0g_{9/2}^{-4})_{J_v}$ predominates with $J_v = 2$ to 12 except for the $23/2_1^-$ and $27/2_1^-$ states that have the main configurations $\pi(0f_{5/2}^{-1}1p_{3/2}^{-1}1p_{1/2}^{-1})\nu(0g_{9/2}^{-4})$ and $\pi(1p_{3/2}^{-1})\nu(0g_{9/2}^{-4})$, respectively. This means that these states are mainly generated by recoupling the neutron spins and coupling the resulting J_v to the spin of the proton in the (fp) subshell. We note that this result is contrary to the configuration proposed for the $13/2_1^-$ to $21/2_1^-$ states in Refs. [34,37] that includes the unlikely excitation of a neutron from an (fp) orbit to the $0g_{9/2}$ orbit just discussed. In the states with higher spins a proton pair is broken and two protons are lifted to $0g_{9/2}$ orbits, resulting in main configurations of the types $\pi(0f_{5/2}^{-2}1p_{3/2}^{-1}0g_{9/2}^2)\nu(0g_{9/2}^{-4})$ or $\pi(0f_{5/2}^{-3}0g_{9/2}^2)\nu(0g_{9/2}^{-4})$. The detailed assignment of the various close-lying calculated states of a given spin to the corresponding experimental states is difficult. The comparison of transition strengths between formally numbered experimental and calculated states as given in Table III may therefore not be meaningful.

In particular for a discussion of the $M1$ sequence D we have grouped states with equal configurations into one sequence instead of the formal assignment just discussed. The states selected in this way are consequently connected by transitions of relatively large strengths as found in the experiment. The resulting level sequence is compared with sequence D in Fig. 7. As can be seen, the sequence of the calculated states is even more irregular than the experimental sequence D and shows a rather doubletlike structure. The states up to $J = 27/2$ have

the main configuration $\pi(1p_{3/2}^{-1})\nu(0g_{9/2}^{-4})_{J_v}$ with $J_v = 6, 8$ up to $J = 19/2$ and $J_v = 10, 12$ from $J = 21/2$ to $J = 27/2$, which indicates the breakup of a second $0g_{9/2}$ neutron pair at $J = 21/2$. The four $0g_{9/2}$ neutrons are fully aligned in the states with $J = 25/2$ and $27/2$ but couple differently to the $1p_{3/2}$ proton hole. This explains the small $B(M1, 25/2_3^- \rightarrow 23/2_2^-)$ value and the nearly degenerate level energies of the $25/2_3^-$ and $27/2_1^-$ states that are not consistent with the experimental findings and may indicate a stronger mixing of the configurations in the experimental $23/2_2^-$ and $25/2_3^-$ states than predicted in the calculations. The $B(M1)$ values between the states from $J = 17/2$ to $23/2$ reproduce roughly the experimental ones with the exception of the $B(M1, 17/2_2^- \rightarrow 15/2_2^-)$ value. An alternative selection for the states up to $J = 27/2$ is the sequence of states with the main configuration $\pi(0f_{5/2}^{-1})\nu(0g_{9/2}^{-4})$. This configuration leads to smaller $B(M1)$ values compared with the ones predicted by the discussed configuration including the unpaired proton in the $1p_{3/2}$ orbit. Because the smaller $B(M1)$ values are at greater variance with the experimental ones, we favor the configuration with the $\pi(1p_{3/2}^{-1})$ orbit. The configuration changes between the calculated $J = 27/2$ and $J = 29/2$ states. This change results in very small $B(M1, 29/2_2^- \rightarrow 27/2_1^-)$, $B(E2, 29/2_2^- \rightarrow 25/2_3^-)$, and $B(E2, 31/2_2^- \rightarrow 27/2_1^-)$ values. These small values are not consistent with the experimental ones, which may indicate that those states have configurations that are more complex than the ones possible in the present configuration space, hence leading to contributions of equivalent components in the states below and above $J = 27/2$.

The predicted main configuration of the states with $J \geq 29/2$ is $\pi(0f_{5/2}^{-2}1p_{3/2}^{-1}0g_{9/2}^2)_{21/2}\nu(0g_{9/2}^{-4})_{J_v}$ with $J_v = 4$ to 8 . This $5qp$ configuration is analogous to the $4qp$ configuration

$\pi(0f_{5/2}^{-2}1p_{3/2}^{-1}0g_{9/2}^2) \nu(0g_{9/2}^{-3})$ predicted by shell-model calculations as well as by TAC-model calculations for the $M1$ band in the neighboring isotope ^{84}Rb [33]. The difference is that the states of the $M1$ band in ^{84}Rb are generated by recoupling the total spin of the protons and the spin of the single unpaired neutron, which corresponds to the shears mechanism, whereas the states of the $M1$ sequence in ^{83}Rb are generated also by recoupling the spins of the two unpaired neutrons only. This resembles a particular possible coupling mode that leads to an irregular $M1$ sequence as described in a shell-model investigation of $M1$ bands in indium isotopes [27]. Thus, this particular spin coupling may be the reason of the loss of regularity in the $M1$ sequence observed in ^{83}Rb . The shears mechanism may then be realized when the spins of the protons and the spins of the neutrons are fully aligned and the “blades” formed by the total proton spin and the total neutron spin start to recouple, i.e., above $J = 43/2$. The calculated $B(M1)$ and $B(E2)$ values between the states from $J = 29/2$ to $37/2$ are in good agreement with the experimental values. This proves that large $M1$ transition strengths at high spin are generated by the recoupling of the spins of the particle-like protons and holelike neutrons in high- j orbits and in addition of nucleons in low- j orbits.

V. CONCLUSIONS

Excited states in the odd-even nuclide $^{83}\text{Rb}_{46}$ were studied with the spectrometer GASP. The level scheme was extended up to an excitation energy of 13.9 MeV and a tentative spin of $49/2$. A large number of mean level lifetimes was determined in addition to previous work. The negative-parity

sequence including relatively strong $M1$ transitions as well as crossover $E2$ transitions turns out to be irregular in contrast to analogous sequences in the neighboring odd-odd isotopes $^{82}\text{Rb}_{45}$ and $^{84}\text{Rb}_{47}$. This indicates that the shears mechanism proposed for the regular $M1$ bands in the neighboring isotopes cannot be realized in the $M1$ sequence in $^{83}\text{Rb}_{46}$. Shell-model calculations predict a configuration for the $M1$ sequence above $J^\pi = 29/2^-$ that is analogous to the configuration predicted by the shell model as well as by the TAC model for the $M1$ shears band in ^{84}Rb and reproduces the order of the experimental $B(M1)$ values. In contrast to the $M1$ band in the neighbor ^{84}Rb , the states in the $M1$ band in ^{83}Rb are also generated by recoupling the individual neutron spins that dilutes the shears mechanism. The shell model with the present restricted configuration does, however, not reproduce the regularity of the $M1$ band in the neighbor ^{84}Rb . A general improvement of the description of shears bands may be achieved by using large-scale or Monte Carlo shell-model calculations with appropriate effective interactions for this mass region.

ACKNOWLEDGMENTS

This work was supported by the European Commission within the TMR/LSF program under Contract No. ERBFMGECT980110. R.S. and G.R. acknowledge financial support by the NATO Grant No. PST.CLG.977744. A.J. acknowledges support from the Spanish Ministerio de Ciencia e Innovación (within the projects FPA2005-00696 and FPA2007-66069) and the Spanish Consolider-Ingenio 2010 Program CPAN (CSD2007-00042).

-
- [1] L. Funke, F. Dönau, J. Döring, P. Kemnitz, E. Will, G. Winter, L. Hildingsson, A. Johnson, and Th. Lindblad, *Phys. Lett.* **B120**, 301 (1983).
 - [2] L. Funke, J. Döring, P. Kemnitz, E. Will, G. Winter, A. Johnson, L. Hildingsson, and Th. Lindblad, *Nucl. Phys.* **A455**, 206 (1986).
 - [3] R. Schwengner, J. Döring, L. Funke, G. Winter, A. Johnson, and W. Nazarewicz, *Nucl. Phys.* **A509**, 550 (1990).
 - [4] P. Kemnitz, J. Döring, L. Funke, G. Winter, L. H. Hildingsson, D. Jerrestam, A. Johnson, and Th. Lindblad, *Nucl. Phys.* **A456**, 89 (1986).
 - [5] J. Döring, L. Funke, G. Winter, F. Lidén, B. Cederwall, A. Johnson, R. Wyss, J. Nyberg, and G. Sletten, in *Proceedings of the International Conference on High Spin Physics and Gamma-soft Nuclei, Pittsburgh, 1990*, edited by J. X. Saladin, R. A. Sorensen, and C. M. Vincent (World Scientific, Singapore, 1991), p. 381.
 - [6] J. Döring, L. Funke, R. Schwengner, and G. Winter, *Phys. Rev. C* **48**, 2524 (1993).
 - [7] R. Schwengner, J. Döring, L. Funke, H. Rotter, G. Winter, A. Johnson, and A. Nilsson, *Nucl. Phys.* **A486**, 43 (1988).
 - [8] R. Schwengner, F. Dönau, T. Servene, H. Schnare, J. Reif, G. Winter, L. Käubler, H. Prade, S. Skoda, J. Eberth, H. G. Thomas, F. Becker, B. Fiedler, S. Freund, S. Kasemann, T. Steinhardt, O. Thelen, T. Härtlein, C. Ender, F. Köck, P. Reiter, and D. Schwalm, *Phys. Rev. C* **65**, 044326 (2002).
 - [9] L. Funke, J. Döring, P. Kemnitz, P. Ojeda, R. Schwengner, E. Will, G. Winter, A. Johnson, L. Hildingsson, and Th. Lindblad, *Z. Phys. A* **324**, 127 (1986).
 - [10] J. W. Holcomb, J. Döring, T. Glasmacher, G. D. Johns, T. D. Johnson, M. A. Riley, P. C. Womble, and S. L. Tabor, *Phys. Rev. C* **48**, 1020 (1993).
 - [11] J. Döring, R. Schwengner, L. Funke, H. Rotter, G. Winter, B. Cederwall, F. Lidén, A. Johnson, A. Atac, J. Nyberg, and G. Sletten, *Phys. Rev. C* **50**, 1845 (1994).
 - [12] R. Schwengner, H. Schnare, S. Frauendorf, F. Dönau, L. Käubler, H. Prade, E. Grosse, A. Jungclaus, K. P. Lieb, C. Lingk, S. Skoda, J. Eberth, G. de Angelis, A. Gadea, E. Farnea, D. R. Napoli, C. A. Ur, and G. Lo Bianco, in *Proceedings of the 2nd International Conference on Exotic Nuclei and Atomic Masses, ENAM98, Bellaire, Michigan, 23–27 June 1998*, AIP Conf. Proc. 455, edited by B. M. Sherrill, D. J. Morrissey, and C. N. Davids (AIP, Woodbury, New York, 1998), p. 594.
 - [13] R. Schwengner, G. Winter, J. Reif, H. Prade, L. Käubler, R. Wirowski, N. Nicolay, S. Albers, S. Eßer, P. von Brentano, and W. Andrejtscheff, *Nucl. Phys.* **A584**, 159 (1995).
 - [14] B. Fant, R. J. Tanner, P. A. Butler, A. N. James, G. D. Jones, R. J. Poynter, C. A. White, K. L. Ying, D. J. G. Love, J. Simpson, and K. A. Connell, *J. Phys. G* **17**, 319 (1991).
 - [15] R. M. Clark, R. Wadsworth, E. S. Paul, C. W. Beausang, I. Ali, A. Astier, D. M. Cullen, P. J. Dagnall, P. Fallon, M. J. Joyce,

- M. Meyer, N. Redon, P. H. Regan, W. Nazarewicz, and R. Wyss, *Phys. Lett.* **B275**, 247 (1992).
- [16] G. Baldsiefen, H. Hübel, D. Mehta, B. V. Thirumala Rao, U. Birkental, G. Fröhlingsdorf, M. Neffgen, N. Nenoff, S. C. Pancholi, N. Singh, W. Schmitz, K. Theine, P. Willsau, H. Grawe, J. Heese, H. Kluge, K. H. Maier, M. Schramm, R. Schubart, and H. J. Maier, *Phys. Lett.* **B275**, 252 (1992).
- [17] A. Kuhnert, M. A. Stoyer, J. A. Becker, E. A. Henry, M. J. Brinkman, S. W. Yates, T. F. Wang, J. A. Cizewski, F. S. Stephens, M. A. Deleplanque, R. M. Diamond, A. O. Macchiavelli, J. E. Draper, F. Azaiez, W. H. Kelly, and W. Korten, *Phys. Rev. C* **46**, 133 (1992).
- [18] R. M. Clark, R. Wadsworth, E. S. Paul, C. W. Beausang, I. Ali, A. Astier, D. M. Cullen, P. J. Dagnall, P. Fallon, M. J. Joyce, M. Meyer, N. Redon, P. H. Regan, J. F. Sharpey-Schafer, W. Nazarewicz, and R. Wyss, *Nucl. Phys.* **A562**, 121 (1993).
- [19] G. Baldsiefen, H. Hübel, W. Korten, D. Mehta, N. Nenoff, B. V. Thirumala Rao, P. Willsau, H. Grawe, J. Heese, K. H. Maier, R. Schubart, S. Frauendorf, and H. J. Maier, *Nucl. Phys.* **A574**, 521 (1994).
- [20] M. Neffgen, G. Baldsiefen, S. Frauendorf, H. Grawe, J. Heese, H. Hübel, H. Kluge, A. Korichi, W. Korten, K. H. Maier, D. Mehta, J. Meng, N. Nenoff, M. Piiparinen, M. Schönhofer, R. Schubart, U. J. van Severen, N. Singh, G. Sletten, B. V. Thirumala Rao, and P. Willsau, *Nucl. Phys.* **A595**, 499 (1995).
- [21] R. M. Clark, S. J. Asztalos, G. Baldsiefen, J. A. Becker, L. Bernstein, M. A. Deleplanque, R. M. Diamond, P. Fallon, I. M. Hibbert, H. Hübel, R. Krücken, I. Y. Lee, A. O. Macchiavelli, R. W. MacLeod, G. Schmid, F. S. Stephens, K. Vetter, R. Wadsworth, and S. Frauendorf, *Phys. Rev. Lett.* **78**, 1868 (1997).
- [22] R. M. Clark and A. O. Macchiavelli, *Annu. Rev. Nucl. Part. Sci.* **50**, 1 (2000).
- [23] S. Frauendorf, *Nucl. Phys.* **A557**, 259c (1993).
- [24] S. Frauendorf, J. Meng, and J. Reif, LBL Report No. LBL35687, 1994.
- [25] S. Frauendorf, *Z. Phys. A* **358**, 163 (1997).
- [26] A. Gadea, G. de Angelis, C. Fahlander, M. DePoli, E. Farnea, T. Li, D. R. Napoli, Q. Pan, P. Spolaore, D. Bazzacco, S. M. Lenzi, S. Lunardi, C. M. Petrache, F. Brandolini, P. Pavan, C. Alvarez, S. Sferrazza, P. G. Bizetti, A. M. Bizetti Sona, J. Nyberg, M. Lipoglavsek, J. Persson, J. Cederkäll, D. Seweryniak, A. Johnson, H. Grawe, F. Soramel, M. Ogawa, A. Makishima, R. Schubart, and S. Frauendorf, *Phys. Rev. C* **55**, R1 (1997).
- [27] S. Frauendorf and J. Reif, *Nucl. Phys.* **A621**, 736 (1997).
- [28] D. G. Jenkins, I. M. Hibbert, C. M. Parry, R. Wadsworth, D. B. Fossan, G. J. Lane, J. M. Sears, J. F. Smith, R. M. Clark, R. Krücken, I. Y. Lee, A. O. Macchiavelli, V. P. Janzen, J. Cameron, and S. Frauendorf, *Phys. Lett.* **B428**, 23 (1998).
- [29] D. G. Jenkins, R. Wadsworth, J. Cameron, R. M. Clark, D. B. Fossan, I. M. Hibbert, V. P. Janzen, R. Krücken, G. J. Lane, I. Y. Lee, A. O. Macchiavelli, C. M. Parry, J. M. Sears, J. F. Smith, and S. Frauendorf, *Phys. Rev. C* **58**, 2703 (1998).
- [30] R. M. Clark, S. J. Asztalos, B. Busse, C. J. Chiara, M. Cromaz, M. A. Deleplanque, R. M. Diamond, P. Fallon, D. B. Fossan, D. G. Jenkins, S. Juutinen, N. Kelsall, R. Krücken, G. J. Lane, I. Y. Lee, A. O. Macchiavelli, R. W. MacLeod, G. Schmid, J. M. Sears, J. F. Smith, F. S. Stephens, K. Vetter, R. Wadsworth, and S. Frauendorf, *Phys. Rev. Lett.* **82**, 3220 (1999).
- [31] F. Brandolini, M. Ionescu-Bujor, N. H. Medina, R. V. Ribas, D. Bazzacco, M. De Poli, P. Pavan, C. Rossi-Alvarez, G. de Angelis, S. Lunardi, D. De Acuña, D. R. Napoli, and S. Frauendorf, *Phys. Lett.* **B388**, 468 (1996).
- [32] H. Schnare, R. Schwengner, S. Frauendorf, F. Dönau, L. Käubler, H. Prade, A. Jungclaus, K. P. Lieb, C. Lingk, S. Skoda, J. Eberth, G. de Angelis, A. Gadea, E. Farnea, D. R. Napoli, C. A. Ur, and G. Lo Bianco, *Phys. Rev. Lett.* **82**, 4408 (1999).
- [33] R. Schwengner, G. Rainovski, H. Schnare, A. Wagner, F. Dönau, A. Jungclaus, M. Hausmann, O. Iordanov, K. P. Lieb, D. R. Napoli, G. de Angelis, M. Axiotis, N. Marginean, F. Brandolini, and C. Rossi Alvarez, *Phys. Rev. C* **66**, 024310 (2002).
- [34] W. Gast, K. Dey, A. Gelberg, U. Kaup, F. Paar, R. Richter, K. O. Zell, and P. von Brentano, *Phys. Rev. C* **22**, 469 (1980).
- [35] J. Döring, G. D. Johns, R. A. Kaye, M. A. Riley, and S. L. Tabor, *Phys. Rev. C* **60**, 014314 (1999).
- [36] S. Ganguly, P. Banerjee, I. Ray, R. Kshetri, S. Bhattacharya, M. Saha-Sarkar, A. Goswami, S. Muralithar, R. P. Singh, R. Kumar, and R. K. Bhowmik, *Nucl. Phys.* **A768**, 43 (2006).
- [37] Amita, A. K. Jain, V. I. Dimitrov, and S. G. Frauendorf, *Phys. Rev. C* **64**, 034308 (2001).
- [38] R. Schwengner, H. Schnare, S. Frauendorf, F. Dönau, L. Käubler, H. Prade, E. Grosse, A. Jungclaus, K. P. Lieb, C. Lingk, S. Skoda, J. Eberth, G. de Angelis, A. Gadea, E. Farnea, D. R. Napoli, C. A. Ur, and G. Lo Bianco, *J. Res. Natl. Inst. Stand. Technol.* **105**, 133 (2000).
- [39] R. Schwengner, G. Rainovski, H. Schnare, A. Wagner, F. Dönau, M. Hausmann, O. Iordanov, A. Jungclaus, K. P. Lieb, D. R. Napoli, G. de Angelis, M. Axiotis, N. Marginean, F. Brandolini, and C. Rossi Alvarez, *Int. Symp. on Nuclear Structure Physics, Göttingen, March 2001*, edited by R. Casten, J. Jolie, U. Kneissl, and P. Lieb (World Scientific, Singapore, 2001), p. 397.
- [40] D. Bazzacco, in *International Conference on Nuclear Structure at High Angular Momentum, Ottawa, 1992* (AECL Research, Chalk River, 1992), p. 386
- [41] D. C. Radford, *Nucl. Instrum. Methods A* **361**, 297 (1995).
- [42] J. Theuerkauf, S. Esser, S. Krink, M. Luig, N. Nicolay, and H. Wolters, Program VS (version 6.65), Universität zu Köln, 1992.
- [43] R. M. Steffen and K. Alder, in *The Electromagnetic Interaction in Nuclear Spectroscopy*, edited by W. D. Hamilton (North-Holland, Amsterdam, 1975), p. 505.
- [44] K. S. Krane, R. M. Steffen, and R. M. Wheeler, *At. Data Nucl. Data Tables* **11**, 351 (1973).
- [45] A. Krämer-Flecken, T. Morek, R. M. Lieder, W. Gast, G. Hebbinghaus, H. M. Jäger, and W. Urban, *Nucl. Instrum. Methods A* **275**, 333 (1989).
- [46] G. Winter, *Nucl. Instrum. Methods* **214**, 537 (1983).
- [47] J. Lindhard, V. Nielsen, and M. Scharff, *Mat. Fys. Medd. K. Dan. Vidensk. Selsk.* **36**, 1 (1968).
- [48] G. Winter, J. Döring, F. Dönau, and L. Funke, *Z. Phys. A* **334**, 415 (1989).
- [49] G. Winter, R. Schwengner, J. Reif, H. Prade, J. Döring, R. Wirowski, N. Nicolay, P. von Brentano, H. Grawe, and R. Schubart, *Phys. Rev. C* **49**, 2427 (1994).
- [50] R. Schwengner, J. Reif, H. Schnare, G. Winter, T. Servene, L. Käubler, H. Prade, M. Wilhelm, A. Fitzler, S. Kasemann, E. Radermacher, and P. von Brentano, *Phys. Rev. C* **57**, 2892 (1998).

- [51] U. I. Zhovliiev, V. G. Kiptilyi, M. F. Kudoyarov, I. Kh. Lemberg, A. I. Muminov, A. A. Pasternak, and L. A. Rassadin, *Izv. Akad. Nauk SSSR, Ser. Fiz.* **49**, 2096 (1985) [*Bull. Acad. Sci. USSR, Phys. Ser.* **49**, No. 11, 13 (1985)].
- [52] P. M. Endt, *At. Data Nucl. Data Tables* **23**, 547 (1979).
- [53] S. Frauendorf, J. Reif, and G. Winter, *Nucl. Phys.* **A601**, 41 (1996).
- [54] S. Frauendorf, *Rev. Mod. Phys.* **73**, 463 (2001).
- [55] R. Schwengner, D. L. Balabanski, G. Neyens, N. Benouaret, D. Borremans, N. Coulier, M. De Rydt, G. Georgiev, S. Mallion, G. Rainovski, G. Rusev, S. Teughels, and K. Vyvey, *Phys. Rev. C* **74**, 034309 (2006).
- [56] G. Winter, R. Schwengner, J. Reif, H. Prade, L. Funke, R. Wirowski, N. Nicolay, A. Dewald, P. von Brentano, H. Grawe, and R. Schubart, *Phys. Rev. C* **48**, 1010 (1993).
- [57] J. Reif, G. Winter, R. Schwengner, H. Prade, L. Käubler, *Nucl. Phys.* **A587**, 449 (1995).
- [58] E. A. Stefanova, R. Schwengner, J. Reif, H. Schnare, F. Dönau, M. Wilhelm, A. Fitzler, S. Kasemann, P. von Brentano, and W. Andrejtscheff, *Phys. Rev. C* **62**, 054314 (2000).
- [59] A. Jungclaus, D. Kast, K. P. Lieb, C. Teich, M. Weiszflog, T. Härtlein, C. Ender, F. Köck, D. Schwalm, J. Reif, R. Peusquens, A. Dewald, J. Eberth, H. G. Thomas, M. Górska, H. Grawe, *Nucl. Phys.* **A637**, 346 (1998).
- [60] A. Jungclaus, D. Kast, K. P. Lieb, C. Teich, M. Weiszflog, T. Härtlein, C. Ender, F. Köck, D. Schwalm, I. P. Johnstone, J. Reif, R. Schwengner, R. Peusquens, A. Dewald, J. Eberth, H. G. Thomas, M. Górska, and H. Grawe, *Phys. Rev. C* **60**, 014309 (1999).
- [61] E. A. Stefanova, R. Schwengner, G. Rainovski, K. D. Schilling, A. Wagner, F. Dönau, E. Galindo, A. Jungclaus, K. P. Lieb, O. Thelen, J. Eberth, D. R. Napoli, C. A. Ur, G. de Angelis, M. Axiotis, A. Gadea, N. Marginean, T. Martinez, Th. Kröll, and T. Kutsarova, *Phys. Rev. C* **63**, 064315 (2001).
- [62] G. Rainovski, R. Schwengner, K. D. Schilling, A. Wagner, A. Jungclaus, E. Galindo, O. Thelen, D. R. Napoli, C. A. Ur, G. de Angelis, M. Axiotis, A. Gadea, N. Marginean, T. Martinez, and Th. Kröll, *Phys. Rev. C* **65**, 044327 (2002).
- [63] E. A. Stefanova, M. Danchev, R. Schwengner, D. L. Balabanski, M. P. Carpenter, M. Djongolov, S. M. Fischer, D. J. Hartley, R. V. F. Janssens, W. F. Mueller, D. Nisius, W. Reviol, L. L. Riedinger, and O. Zeidan, *Phys. Rev. C* **65**, 034323 (2002).
- [64] D. Rudolph, K. P. Lieb, and H. Grawe, *Nucl. Phys.* **A597**, 298 (1996).
- [65] E. Galindo, A. Jungclaus, and K. P. Lieb, *Eur. Phys. J. A* **9**, 439 (2000).
- [66] X. Ji and B. H. Wildenthal, *Phys. Rev. C* **37**, 1256 (1988).
- [67] R. Gross and A. Frenkel, *Nucl. Phys.* **A267**, 85 (1976).
- [68] J. Blomqvist and L. Rydström, *Phys. Scr.* **31**, 31 (1985).
- [69] D. H. Gloeckner and F. J. D. Serduke, *Nucl. Phys.* **A220**, 477 (1974).
- [70] D. Zwarts, *Comput. Phys. Commun.* **38**, 365 (1985).